Variable Beamwidth Near Field Codebook Design for Communications Aided by A Large Scale RIS

Xiaowen Tian[†], Nuria Gonzalez-Prelcic[†], Robert W. Heath Jr.[†]

**Electrical and Computer Engineering Department

*North Carolina State University

Raleigh, NC, 27606, USA

E-mail: {xtian8, ngprelcic, rwheathjr}@ncsu.edu

Abstract—Reconfigurable intelligent surfaces (RISs)-aided communication at millimeter wave frequencies will likely require a large size RIS to achieve the expected link budget in outdoor environments. This large size of the RIS will induce a near field (NF) operation mode. Previous approaches to operate in the NF consider RIS configurations that provide very focused beams, targeted toward a grid of user locations to build the corresponding codebook. In this paper, we design variable width beam codebooks for the NF using a technique that maps the RIS elements to a tunable spherical surface. By tuning the size and center of the surface, variable width beams and illuminated areas can be achieved. Simulation results show the effectiveness of the proposed method to maintain a high average rate while expanding the illumination region associated to beam focusing. Our configuration also outperforms the state-of-the-art in terms of maintaining the intended shape of the illuminated region even if not in the boresight directions of the RIS.

Index Terms—Variable beamwidth, near field (NF), codebook, large scale RIS, mmWave communication.

I. INTRODUCTION

Electrically large reconfigurable intelligent surfaces (RISs) may be needed to operate at millimeter wave (mmWave) frequencies, or when large coverage areas are intended. The large size of the RIS means that communication is more likely to be in the near field (NF). Effective designs for the configuration of the RIS under the far field (FF) assumption [1]–[3], though, will lead to performance losses if the RIS is actually operating in the NF.

Recent work has considered the configuration of RIS in the NF, with an emphasis on beam focusing designs. An optimal NF beam focusing configuration was proposed in [4] so that the received power is maximized for a given location. Some beam codebook designs to provide beam focusing when operating in the NF with a large RIS were proposed in [5]–[7]. They provide extremely focused beam patterns that offer a high gain but are not robust to user location errors. Moreover, since each codeword contains a very narrow beam, a large size codebook is required to cover an intended region of interest, which significantly increases the configuration overhead. Although the beam width of each codeword could be increased by muting certain RIS elements, deactivating the

This material is based upon work partially supported by the National Science Foundation under grant no. NSF-CNS-2147955 and is supported in part by funds from federal agency and industry partners as specified in the Resilient & Intelligent NextG Systems (RINGS) program.

elements reduces the array gain. Therefore, it is interesting to design RIS configuration methods that can create wider beam patterns, or in general, variable width beam patterns, while keeping a reasonable gain.

To the best of our knowledge, the only variable beamwidth RIS configuration for NF operation considering a rectangular RIS was proposed in [8], [9]. The design is based on the definition of a mapping function to determine an expanded rectangular illumination region around the target user equipment (UE). In this case, the RIS configuration is determined by the relative locations of each RIS element with respect to the center of the RIS. Although the intended illumination region is rectangular, this design does not guarantee the expected shape and size, especially when the target UEs are away from the boresight of the RIS. As such, that RIS configuration works reasonably well only for a limited range of the UEs locations.

In this paper, we make two main contributions to the design of variable beamwidth RISs for NF operation. First, we propose a novel RIS configuration design based on mapping the locations of all RIS elements to a predefined spherical surface, which allows for variable beamwidth control. This design outperforms previous RIS configurations [8], [9] in terms of maintaining the desired shape of the illumination region while achieving a high average rate. Second, we propose a codebook design that exploits the proposed spherical mapping to obtain variable beamwidth codewords. Our simulation results demonstrate the effectiveness of our proposed approach in expanding the illumination region while maintaining a high average rate, outperforming state-of-the-art NF RIS configurations.

II. NEAR FIELD SYSTEM MODEL

We consider a RIS-assisted downlink system, where the base station (BS) and the UE are working in the NF of a RIS, as shown in Fig. 1. The UE is on the xy-plane, and the RIS is located at a height z on the yz-plane, facing the direction of the positive x-axis. The total number of RIS elements is denoted as Q. The locations of the BS, UE, and the i-th RIS element are represented by \mathbf{p}_{BS} , \mathbf{p}_{UE} and \mathbf{p}_i . The distance between the BS and the i-th RIS element is $d_{1,i} = \|\mathbf{p}_{\mathrm{BS}} - \mathbf{p}_i\|$, and the corresponding elevation angle is $\psi_{1,i} \in [0, \frac{\pi}{2}]$. Similarly, the distance between the UE and the i-th RIS element is $d_{2,i} = \|\mathbf{p}_{\mathrm{UE}} - \mathbf{p}_i\|$, and the elevation angle is $\psi_{2,i} \in [0, \frac{\pi}{2}]$.

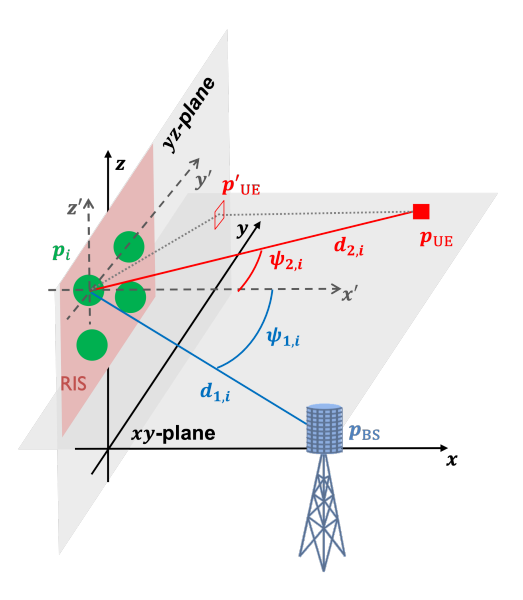


Fig. 1. The system model of a RIS-assisted downlink. The UE is on the xy-plane, and the RIS is on the yz-plane facing the direction of the positive x-axis. The BS, UE, and i-th RIS element locations are \mathbf{p}_{BS} , \mathbf{p}_{UE} and \mathbf{p}_i . The distance between BS and the i-th RIS element is $d_{1,i} = \|\mathbf{p}_{\mathrm{BS}} - \mathbf{p}_i\|$, and the elevation angle is $\psi_{1,i}$. Similarly, the distance between the UE and the i-th RIS element is $d_{2,i} = \|\mathbf{p}_{\mathrm{UE}} - \mathbf{p}_i\|$, and the elevation angle is $\psi_{2,i}$.

We assume that the BS-UE link is blocked, but the link BS-RIS-UE can be established. We consider operation in the NF at mmWave frequencies, and we model the *effective* channel (including the impact of BS and UE beamforming) between the BS and the i-th RIS element, $h_{1,i}$, as a single-path line-of-sight (LoS) link, which can be written as a function of the signal travel distance $d_{1,i}$ as

$$h_{1,i} = \frac{\sqrt{F_{1,i}}}{d_{1,i}} e^{-j\frac{2\pi}{\lambda}d_{1,i}} \tag{1}$$

Analogously, we can write the channel between the UE and the i-th RIS element as $h_{2,i}=\frac{\sqrt{F_{2,i}}}{d_{2,i}}e^{-j\frac{2\pi}{\lambda}d_{2,i}}$. The effect of the phase shift configuration of the i-th RIS element is denoted as

$$h_i = e^{j\phi_i}. (2)$$

where we assume that the reflection coefficient is 1 and ϕ_i is the phase of *i*-th RIS element.

Leveraging the NF-model in [4], the received signal is

$$y = \sqrt{\alpha} \sum_{i=1}^{Q} h_{2,i} h_i h_{1,i} s + n,$$
 (3)

where α is a gain factor, and y, s and n are the received data, transmitted data, and noise sample, which is modeled as additive white Gaussian noise with zero mean and variance $\sigma_{\rm n}^2$. The gain factor can be defined as $\alpha = P_{\rm t}G_{\rm t}G_{\rm r}G_{\rm RIS}d_{\rm y}d_{\rm z}(\frac{\lambda}{4\pi})^2$, where $P_{\rm t}$ is the BS transmit power, $G_{\rm t}$ is the BS antenna gain, $G_{\rm r}$ is the UE antenna gain, $G_{\rm RIS}$ is the RIS element gain, $d_{\rm y}$ and $d_{\rm z}$ are the sizes of each RIS element on the y-axis

and z-axis, and λ is the wavelength. From the received signal expression, we can obtain the received SNR as

$$\eta = \frac{\alpha}{\sigma_{\rm n}^2} \left| \sum_{i=1}^{Q} \frac{\sqrt{F_{1,i}}}{d_{1,i}} \frac{\sqrt{F_{2,i}}}{d_{2,i}} e^{-j\frac{2\pi}{\lambda}(d_{1,i}+d_{2,i})} e^{j\phi_i} \right|^2, \quad (4)$$

where $F_{j,i} = \cos^3 \psi_{j,i}$, with i = 1, ..., Q, j = 1 for the BS and j = 2 for the UE, is the normalized RIS radiation pattern [4], which only depends on the elevation angles with respect to the *i*-th RIS element. Given this radiation pattern, the RIS element gain can be easily computed as $G_{\text{RIS}} = 8$ [4].

III. PROPOSED VARIABLE BEAMWIDTH RIS CONFIGURATION AND CODEBOOK DESIGN

A. Motivation for NF variable beamwidth configuration

The near-far field boundary is usually described by the Fraunhofer distance [10]

$$D_{\rm FA} = \frac{2D^2}{\lambda},\tag{5}$$

where D is the aperture of the RIS. When operating at mmWave frequencies, this distance can be large, and NF operation must be considered. For example, given a 1 m \times 1 m RIS with the inter-element distance set to half-wavelength, and considering a carrier frequency of 30 GHz, the near-far field boundary is 400 m.

From (4), the optimal RIS configuration for beam focusing in the NF (NFBF) consists of compensating for the phase shift caused by the signal trip, i.e.,

$$\phi_i = \mod\left(\frac{2\pi}{\lambda} \left(d_{1,i} + d_{2,i}\right), 2\pi\right). \tag{6}$$

Under this RIS configuration, the signal reflected by the RIS will be highly focused on the \mathbf{p}_{UE} .

When the transceivers are in the NF of the RIS, the wavefront associated with the signals reaching the transceivers has to be modeled as spherical, not planar [10]. If a far field beamforming (FFBF) configuration, which assumes a planar wavefront [7], is used in the NF scenario, the gain of the RISassisted link will decrease. Therefore, it is essential to design RIS configurations to operate in the NF setting. Solutions based on beam focusing in the NF as in (6) are not the best approach to operate at mmWave though. First, to achieve a high received signal power at mmWave frequencies, a large number of RIS elements is needed, to compensate for the small wavelength. However, larger Q results in narrower beams, which are not robust to slight UE misalignments. Second, the complexity of the initial access and channel estimation procedure will be prohibitive when employing very narrow highly focused beams. Finally, the same RIS may need to serve more than one user, and wider beams may be needed. To overcome these limitations, in this paper, we propose a variable beamwidth RIS configuration in the NF for mmWave systems.

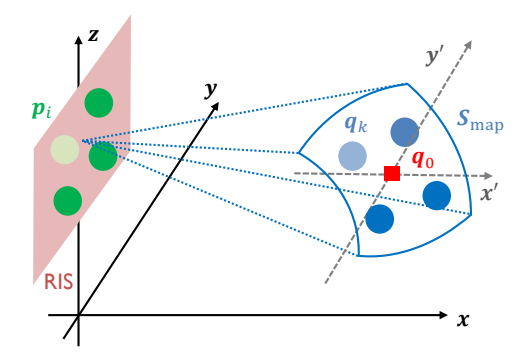


Fig. 2. Illustration of the proposed mapping scheme. The mapping from the i-th RIS element \mathbf{p}_i to the k-th point \mathbf{q}_k on the spherical surface \mathcal{S}_{map} is shown in light colors. The center of the desired region \mathbf{q}_0 is highlighted in red, belonging to both xy-plane and \mathcal{S}_{map} .

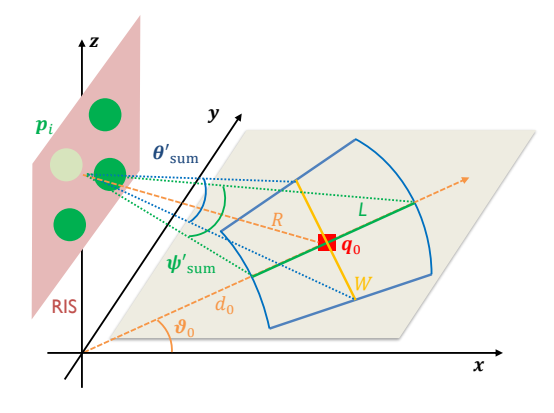


Fig. 3. Illustration of the illuminated area on the xy-plane associated to the sphere \mathcal{S}_{map} on xy-plane. The desired illumination area is marked in blue, with width W, length L, and the center located at \mathbf{q}_0 . The spreading angles of azimuth θ'_{sum} and elevation ψ'_{sum} for this desired illumination shape can be derived from W and L, and the radius of the spherical surface \mathcal{S}_{map} is R, which is the distance between the RIS center and \mathbf{q}_0 .

B. Variable beamwidth RIS configuration

Inspired by the optimal NFBF configuration in (6), where all the Q elements are configured to direct the signals to \mathbf{p}_{UE} , we propose a spherical mapping method to create variable width beams, generally wider than those obtained with NFBF. This way, the Q RIS elements $\bigcup \mathbf{p}_i$ are mapped to Q close points $\bigcup \mathbf{q}_k$ located on a spherical surface $\mathcal{S}_{\mathrm{map}}$, i.e. $\mathbf{q}_k \in \mathcal{S}_{\mathrm{map}}, k = 1, \cdots, Q$, with the same arrangement order as the RIS elements. The mapping procedure is illustrated in Fig. 2, where the center of the desired illumination area on the xy-plane, whose location is denoted as \mathbf{q}_0 , intersects with the 3D spherical surface. In other words, the radius of the spherical surface R is the distance between the RIS center and \mathbf{q}_0 . Assuming that the RIS center is located at $\mathbf{p}_{\mathrm{RIS}} = [0,0,z]$, we have that

$$\mathbf{q}_0 = [R\sin\psi_0\cos\theta_0, R\sin\psi_0\sin\theta_0, R\cos\psi_0 + z], \quad (7)$$

where ψ_i and θ_i represent the elevation and azimuth angle of the point i on the spherical surface \mathcal{S}_{map} with respect to the center of the RIS. The intersect point \mathbf{q}_0 can also be

represented as

$$\mathbf{q}_0 = [d_0 \cos \theta_0, d_0 \sin \theta_0, 0], \tag{8}$$

where d_0 is the distance from \mathbf{q}_0 to the origin, and ϑ_0 is the angle with the x-axis, as illustrated in Fig. 3. Therefore, we can establish the relationships

$$\psi_0 = \arccos\left(\frac{-z}{R}\right), \psi_0 \in \left[\frac{\pi}{2}, \pi\right]$$

$$\theta_0 = \arcsin\left(\frac{d_0 \sin \theta_0}{R \sin \psi_0}\right), \theta_0 \in \left[-\frac{\pi}{2}, \frac{\pi}{2}\right].$$
(9)

With the proposed mapping, the illumination shape on the UE plane will be a circular sector. Therefore, given the length L and width W of the desired illumination region, together with its center \mathbf{q}_0 , we can determine the spherical surface through a simple geometric calculation by obtaining its spreading azimuth and elevation angles, denoted by θ'_{sum} and ψ'_{sum} , which are shown in Fig. 3. Specifically, we obtain

$$\theta'_{\text{sum}} = 2 \arcsin\left(\frac{W}{2d_0}\right),$$

$$\psi'_{\text{sum}} = \left|\arctan\left(\frac{d_0 - \frac{L}{2}}{z}\right) - \arctan\left(\frac{d_0 + \frac{L}{2}}{z}\right)\right|.$$
(10)

To further control the shape of the illuminated area using our proposed configuration, we use an expansion coefficient β that changes the size of the spherical surface by letting

$$\theta_{\text{sum}} = \frac{\theta'_{\text{sum}}}{\beta}, \quad \psi_{\text{sum}} = \frac{\psi'_{\text{sum}}}{\beta}.$$
 (11)

After obtaining the spherical surface S_{map} , we compute the mapped points locations $\bigcup \mathbf{q}_k$ such that the spreading azimuth and elevation angles are evenly divided. Denote N_z and N_y as the number of RIS elements along the z-axis and y-axis, respectively. Then, we map the z-axis RIS elements by assigning different mapped elevation angles as

$$\psi_{k_z} = \frac{\psi_{\text{sum}}}{N_z - 1} (k_z - 1) + \psi_0 - \frac{\psi_{\text{sum}}}{2}, \tag{12}$$

and map the y-axis RIS elements by assigning different mapped azimuth angles as

$$\theta_{k_y} = \frac{\theta_{\text{sum}}}{N_y - 1} (k_y - 1) + \theta_0 - \frac{\theta_{\text{sum}}}{2},$$
 (13)

where k_z and k_y are the indices of the k-th mapped point \mathbf{q}_k , with $k = N_y(k_z - 1) + k_y$, which follows the same mapping order as the RIS elements, whose i-th element location can be expressed by

$$\mathbf{p}_{i} = \left[0, \frac{\lambda}{2} \left(n_{y} - 1 - \frac{N_{y} - \lambda}{2}\right), \frac{\lambda}{2} \left(n_{z} - 1 - \frac{N_{z} - \lambda}{2}\right) + z\right],\tag{14}$$

with n_z and n_y being the indices of the *i*-th mapped point \mathbf{q}_i , with $i = N_y(n_z - 1) + n_y$.

Now, the coordinates of the k-th closely located point on the spherical surface can be computed as

$$\mathbf{q}_k = [R\sin\psi_{k_z}\cos\theta_{k_y}, R\sin\psi_{k_z}\sin\theta_{k_y}, R\cos\psi_{k_z} + z],$$
(15)

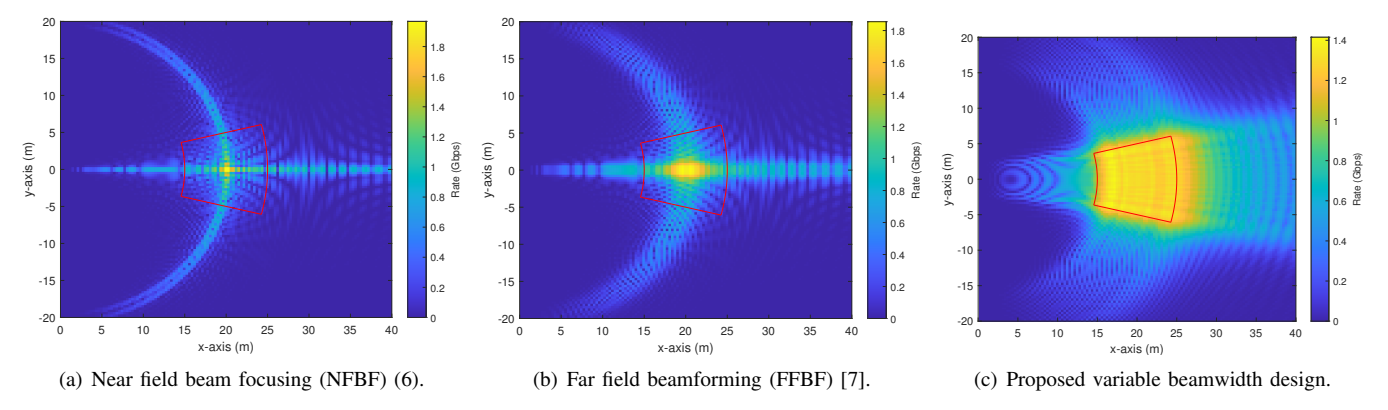


Fig. 4. Rate heatmap comparison of different RIS configurations. The desired illumination region is marked in red, has a length of L=10 m, a width of W=10 m, and is centered at \mathbf{q}_0 . The average rates \widetilde{R} for NFBF, FFBF, and the proposed configuration are 0.44 Gbps, 0.70 Gbps, and 1.29 Gbps.

where $R = \sqrt{d_0^2 + z^2}$ while the other variables are computed as described in (9)-(13). In other words, the mapped point can be obtained by a mapping function $\mathbf{q}_k = f(\mathbf{p}_i, \mathbf{q}_0, \psi_{\text{sum}}'(\text{or }L), \theta_{\text{sum}}'(\text{or }W), \beta)$, which is dependent on the *i*-th RIS element location, the center of the desired illumination region, and the spreading angles of the mapped spherical surface (or the sizes of the illuminated region on the user surface).

Then the proposed variable beamwidth configuration for the i-th RIS element is

$$\phi_{i} = \mod \left(\frac{2\pi}{\lambda} \left(d_{1,i} + d_{2,i,k}\right), 2\pi\right), \tag{16}$$

where $d_{2,i,k} = \|\mathbf{q}_k - \mathbf{p}_i\|$ is the distance from the *i*-th RIS element to the *k*-th mapped point on \mathcal{S}_{map} .

C. Codebook design with variable beamwidth codewords

As discussed in the previous subsection, the shape of the illuminated area on the xy-plane when using the proposed variable beamwidth RIS configuration is a circular sector, determined by the desired length L, width W, expansion coefficient β , and the center location \mathbf{q}_0 . Therefore, a codebook could be designed by determining these four parameters for a given set of codewords. A simple strategy could be to evenly distribute as many center points as the desired number of codewords inside the region of interest, to create subregions of similar size. Then for each subregion, we can adopt the proposed variable beamwidth design in Sec. III-B. Alternatively, we can also obtain each codeword by assigning its center location $\mathbf{q}_0^{(c)}$, and azimuth and elevation spreading angles $\theta_{\text{sum}}^{(c)}$, $\psi_{\text{sum}}^{(c)}$, where c is the index of the codeword and $c=1,\cdots,C$, where C is the codebook size.

IV. SIMULATION RESULTS

We consider the system setup illustrated in Fig. 1. To evaluate our proposed design, we consider that the system operates at 30 GHz, with a bandwidth B=100 MHz, a transmit power $P_{\rm t}=20$ dBm, a BS antenna gain $G_{\rm t}=24$ dB, a UE antenna gain $G_{\rm r}=6$ dB, and a RIS element gain $G_{\rm RIS}=8$. The noise power is calculated as $\sigma_{\rm n}^2=BN_0N_f$,

where $N_0 = -174$ dBm/Hz is the Boltzman constant and $N_f = 6$ dB is the noise factor. The size of the RIS is 1 m \times 1 m with an inter-element spacing of half-wavelength so that the total number of RIS elements is $Q = 200 \times 200$. With this configuration, the size of each RIS element is $d_{\rm V} \times d_{\rm Z} = \lambda/4$.

A. Performance metric

To evaluate the performance of different RIS configuration methods, we use the average rate within a given region of interest, assuming a uniform distribution of the users. Based on the SNR for the u-th user η_u , as defined in (4), and denoting the total number of users within the region of interest as $N_{\rm u}$, the average rate is $\widetilde{R} = \frac{1}{N_{\rm u}} \sum_{u}^{N_{\rm u}} B \log_2(1 + \eta_u)$.

B. Performance of the proposed design

We first illustrate the rate heatmap of our proposed variable beamwidth configuration for RIS with an example system layout and compare the results with those of the NFBF configuration in (6), and the FFBF strategy in [7]. The locations of the BS, the center of the RIS, and the target region center are $\mathbf{p}_{BS} = [30, 0, 30] \text{ m}, \mathbf{p}_{RIS} = [0, 0, 10] \text{ m} \text{ and } \mathbf{q}_0 = [20, 0, 0]$ m. The region of interest has a length of $L=10~\mathrm{m}$ and a width of W = 10 m, and it is centered at q_0 . Under this setting, we adopt an expansion coefficient $\beta = 1.8$ in (11) to control the shape of the illuminated area. Figs. 4 shows the rate heatmaps within a region of size $40 \text{m} \times 40 \text{m}$, whose center is q_0 , highlighted by red boxes. The average rates R for NFBF, FFBF, and the proposed configuration are 0.44 Gbps, 0.70 Gbps, and 1.29 Gbps, respectively. Moreover, it can be seen that both NFBF and FFBF cannot cover the whole desired region, while the proposed variable beamwidth configuration can approximately evenly distribute the power within it. Furthermore, when the RIS has certain muted elements and the number of active elements is $Q = 10 \times 20$, the average rate is 0.39 Gbps. The illuminated region expands but at the cost of a severe gain loss, which leads to performance even worse than NFBF with all active elements. Therefore, our proposed variable beamwidth configuration significantly outperforms both NFBF and FFBF methods.

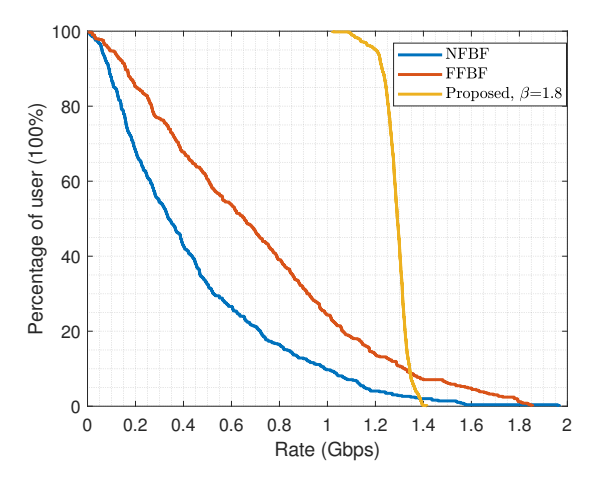


Fig. 5. Percentage of users achieving different rates by comparing NFBF, FFBF, and the proposed configurations.

In Fig. 5, we plot the percentage of users achieving different rates within the same region defined for the example in Figs. 4. We can observe that 50% of the users that use the proposed configuration achieve a rate of around 1.3 Gbps, while that number for NFBF or FFBF decreases to less than 0.65 Gbps. In addition, 95% of the users using the proposed configuration achieve a rate above 1.2 Gbps, while 95% of the users using NFBF or FFBF have a rate above only 0.1 Gbps. Our proposed strategy provides coverage for the whole region of interest approximately evenly and achieves a significant improvement in the average rate over NFBF or FFBF.

To further investigate the ability to achieve variable illumination of the proposed method, we plot the average rate \widetilde{R} versus the size of the interested region in Figs. 6. The proposed RIS configuration has a significant improvement in terms of the average rate with respect to NFBF and FFBF, due to its approximately uniform power distribution within the region of interest, for all considered sizes.

C. Example codebook design

In this section, we create a basic codebook with size C=8. The design of the codebook relies on the design of the codeword center locations \mathbf{q}_0 , and the corresponding expansion azimuth and elevation angles $\theta_{\rm sum}$ and $\psi_{\rm sum}$. In Fig. 7, we set the locations of $\mathbf{q}_0^{(c)}$ as $\mathbf{q}_0^{(c)}=[d^{(c)}\cos\vartheta^{(c)},d^{(c)}\sin\vartheta^{(c)},0]$, for c=1,2,5,6, and $\mathbf{q}_0^{(c)}=[d^{(c)}\cos\vartheta^{(c)},-d^{(c)}\sin\vartheta^{(c)},0]$, for c=3,4,7,8, where $d^{(c)}$ is the distance from $\mathbf{q}_0^{(c)}$ to the origin, and $\vartheta^{(c)}$ is the angle between $\mathbf{q}_0^{(c)}$ and the x-axis. We set $d^{(c)}=d_1=17$ m for c=1,2,3,4, and $d^{(c)}=d_2=23$ m for c=5,6,7,8. $\vartheta^{(c)}=\vartheta_1=15^o$ for c=2,3,6,7, and $\vartheta^{(c)}=\vartheta_2=45^o$ for c=1,4,5,8. The expansion azimuth angles are $\theta_{\rm sum}=15^o$ for all $\mathbf{q}_0^{(c)}$, while the expansion elevation angles are $\psi_{\rm sum}=5^o$ for $\mathbf{q}_0^{(c)},c=1,\cdots,4$ and $\psi_{\rm sum}=3^o$ for $\mathbf{q}_0^{(c)},c=5,\cdots,8$. Since we do not derive the expansion angles from the actual size L or W of each codeword's intended illumination region, it is not necessary to set the expansion coefficient β .

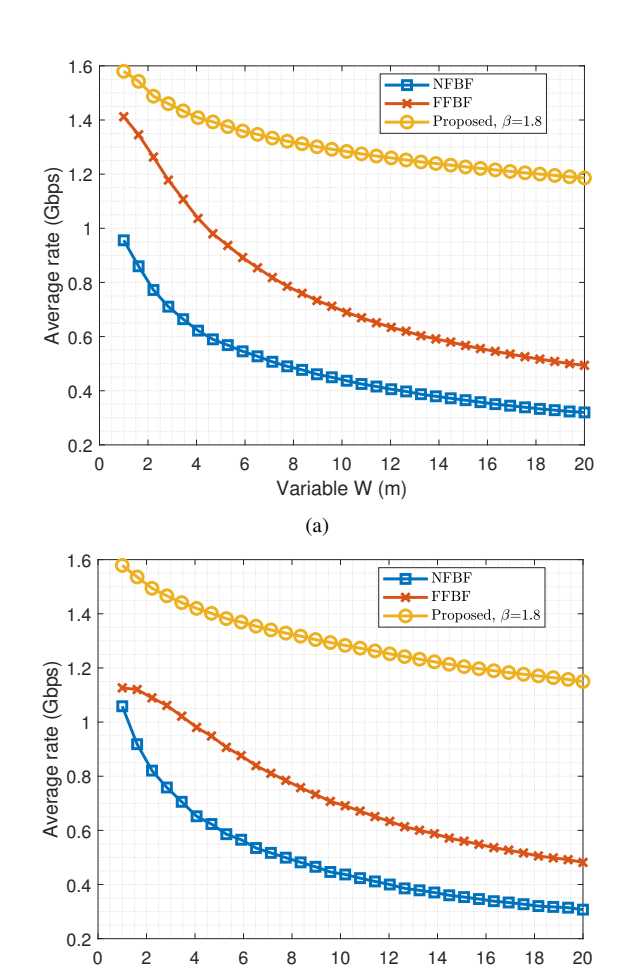


Fig. 6. Average rate comparison: (a) average rate as a function of the width (W) of the region of interest while fixing the length to L=10 m; (b) average rate as a function of the length (L) of the region of interest while fixing the width to W=10 m.

(b)

Variable L (m)

With this codebook design, the covered angular area is as large as $\theta_{\rm cb}=\pm 53^o$, and $d_{\rm cb}=10$ m in width. From Fig. 7, it can be seen that despite the codewords' direction being far from the boresight direction of the RIS, the proposed design still provides good shape control. This example shows that the codebook based on the proposed variable beamwidth RIS configuration can provide good illumination with a smaller codebook size when compared with NFBF or FFBF methods, which cannot control the beamwidth.

D. Comparison with state-of-the-art designs

Fig. 8 shows a comparison of the shape of the illuminated area for an example codeword in [8] [9] and the proposed variable beamwidth configuration. The simulation parameters and the received SNR model are adopted from [8] with BS, RIS, and UE located at $\mathbf{p}_{\mathrm{BS}} = [30, -50, 10]$ m, $\mathbf{p}_{\mathrm{RIS}} = [0, 0, 5]$ m and $\mathbf{p}_{\mathrm{UE}} = [20, 20, 1]$ m. The RIS size is 1 m \times 1 m. The wide beam parameter for generating Fig 8(a) is $\Delta = 8$ m, while the expansion angles for azimuth and elevation for generating Fig. 8(b) are $\theta_{\mathrm{sum}} = 15^o$ and $\psi_{\mathrm{sum}} = 2^o$. It can

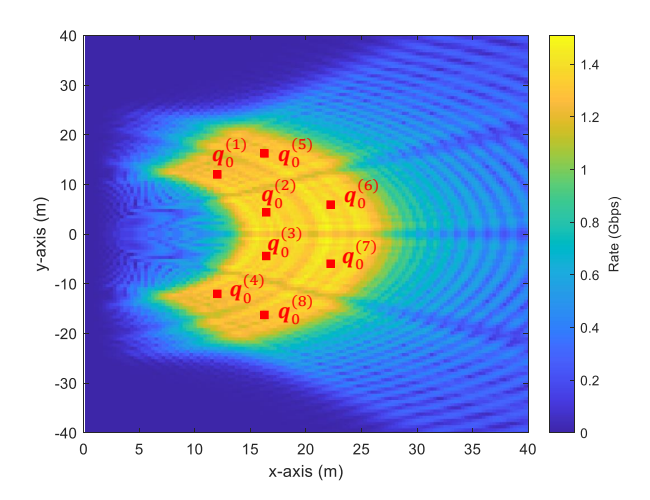


Fig. 7. Rate heatmap of an example codebook design of size C=8. Center positions for each codeword are highlighted with a red square.

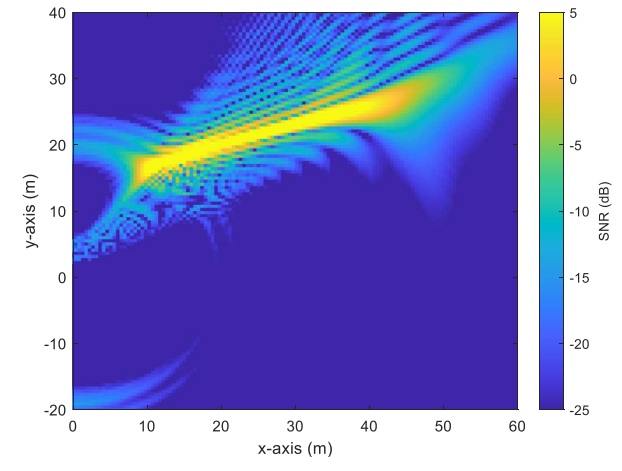
be seen that although the desired shape for the illuminated area in Fig. 8(a) is rectangular, the actual illumination region is significantly off, indicating a limited effective range of UE locations. The proposed variable beamwidth configuration maintains, however, a satisfactory shape of the illuminated area, showing some minimal leakage.

V. CONCLUSION

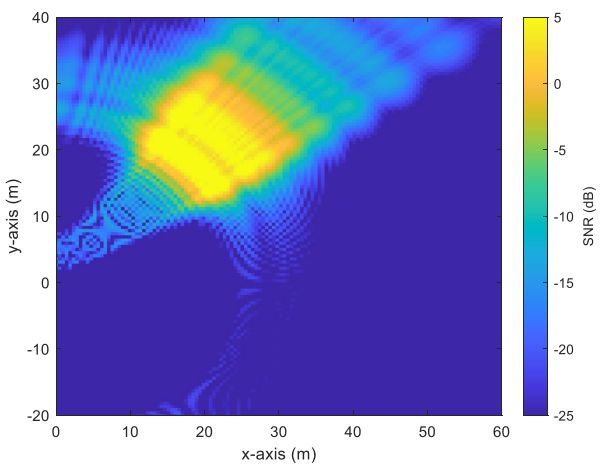
We proposed a variable beamwidth RIS configuration for the NF scenario. The proposed configuration maps the RIS elements to a spherical surface whose radius and spreading angles of azimuth and elevation determine the desired size of the illuminated area. Simulation results showed that, given a region of interest, the proposed configuration achieves a significantly higher average rate than both, NF beam focusing and FF beamforming methods. In addition, we created an example of a codebook that exploits the proposed variable beamwidth design, which can cover a relatively large area with a small number of codewords. Unlike the variable beamwidth configuration method proposed in prior work, our new design can maintain the intended shape of the area being illuminated, even when this region is far from the boresight direction.

REFERENCES

- [1] E. Björnson, H. Wymeersch, B. Matthiesen, P. Popovski, L. Sanguinetti, and E. de Carvalho, "Reconfigurable intelligent surfaces: A signal processing perspective with wireless applications," *IEEE Signal Processing Magazine*, vol. 39, no. 2, pp. 135–158, 2022.
- [2] S. H. Hong, J. Park, S.-J. Kim, and J. Choi, "Hybrid beamforming for intelligent reflecting surface aided millimeter wave MIMO systems," *IEEE Transactions on Wireless Communications*, vol. 21, no. 9, pp. 7343–7357, 2022.
- [3] M. Bayraktar, J. Palacios, N. González-Prelcic, and C. J. Zhang, "Multidimensional orthogonal matching pursuit-based RIS-aided joint localization and channel estimation at mmWave," in 2022 IEEE 23rd International Workshop on Signal Processing Advances in Wireless Communication (SPAWC), 2022, pp. 1–5.
- [4] W. Tang et al., "Wireless communications with reconfigurable intelligent surface: Path loss modeling and experimental measurement," *IEEE Trans. Wireless Commun.*, vol. 20, no. 1, pp. 421–439, 2021.



(a) Variable beamwidth configuration in [8] and [9].



(b) Proposed variable beamwidth configuration (16).

Fig. 8. SNR heatmap of the variable beamwidth configurations adopting the same simulation parameters and received SNR model as in [8], with BS, RIS, and UE located at $\mathbf{p}_{BS} = [30, -50, 10] \text{m}$, $\mathbf{p}_{RIS} = [0, 0, 5] \text{m}$ and $\mathbf{p}_{UE} = [20, 20, 1] \text{m}$. The RIS size is 1 m \times 1 m. The selected wide beam parameter to generate (a) is $\Delta = 8 \text{m}$, while the expansion angles for azimuth and elevation used to generate (b) are $\theta_{\text{sum}} = 15^o$ and $\psi_{\text{sum}} = 2^o$.

- [5] F. Wang, X. Wang, X. Li, X. Hou, L. Chen, S. Suyama, and T. Asai, "Ring-type codebook design for reconfigurable intelligent surface near-field beamforming," in 2022 IEEE PIMRC, Sep. 2022.
- [6] S. Hu, H. Wang, and M. Ilter, "Design of near-field beamforming for large intelligent surfaces," July 2022. [Online]. Available: https://doi.org/10.36227/techrxiv.20334723.v1
- [7] X. Wei, L. Dai, Y. Zhao, G. Yu, and X. Duan, "Codebook design and beam training for extremely large-scale RIS: Far-field or near-field?" *China Communications*, vol. 19, no. 6, pp. 193–204, 2022.
- [8] V. Jamali, G. C. Alexandropoulos, R. Schober, and H. V. Poor, "Low-to-zero-overhead IRS reconfiguration: Decoupling illumination and channel estimation," *IEEE Commun. Letters*, vol. 26, no. 4, pp. 932–936, 2022.
- O] G. C. Alexandropoulos, V. Jamali, R. Schober, and H. V. Poor, "Near-field hierarchical beam management for RIS-enabled millimeter wave multi-antenna systems," in 2022 IEEE 12th Sensor Array and Multi-channel Signal Processing Workshop (SAM), 2022, pp. 460–464.
- [10] E. Bjornson, O. T. Demir, and L. Sanguinetti, "A primer on near-field beamforming for arrays and reconfigurable intelligent surfaces," in 2021 55th Asilomar Conf. on Signals, Systems, and Computers, 2021, pp. 105–112.